ACS SENSORS

Article

Label-free bacterial toxins detection in water supplies using porous silicon nanochannel sensors

Nekane Reta, Andrew Michelmore, Christopher P Saint, Beatriz Prieto-Simon, and Nicolas H. Voelcker

ACS Sens., **Just Accepted Manuscript** • DOI: 10.1021/acssensors.8b01670 • Publication Date (Web): 29 May 2019

Just Accepted

is published by the American Chemical Society. 1155 Sixteenth Street N.W., Washington, DC 20036

Label-free bacterial toxins detection in water supplies using porous silicon nanochannel sensors

Nekane Reta,[a] Andrew Michelmore,[a,c] Christopher P. Saint,[a,b] Beatriz Prieto-Simon,[*,a,d] and Nicolas H. Voelcker[*,a,d,e]

[a] *Future Industries Institute, University of South Australia, Mawson Lakes, South Australia 5095, Australia*

[b] *Natural & Built Environments Research Centre, School of Natural & Built Environments, University of South Australia, Mawson Lakes, South Australia 5095, Australia*

[c] *School of Engineering, University of South Australia, Mawson Lakes, South Australia 5095, Australia*

[d] *Monash Institute of Pharmaceutical Sciences, Monash University, Parkville, Vic 3052, Australia*

[e] *Melbourne Centre for Nanofabrication, Victorian Node of the Australian National Fabrication Facility, Clayton, Victoria, 3168, Australia*

Corresponding authors: Prof. Nicolas H. Voelcker, Dr. Beatriz Prieto-Simon

Drug Delivery, Disposition and Dynamics, Monash Institute of Pharmaceutical Sciences, Monash University, 381 Royal Parade, Parkville, Victoria, 3052, Australia

Tel: +61 3 99039230

email: nicolas.voelcker@monash.edu

beatriz.prieto-simon@monash.edu

Abstract

Lipopolysaccharides (LPS) are the major component of the outer membrane of all Gram-negative bacteria and some cyanobacteria, and are released during growth and cell death. LPS pose a potential health risk in water, causing acute respiratory illnesses, inhalation fever, and gastrointestinal disorders. The need for rapid and accurate detection of LPS has become a major priority to facilitate more timely and efficacious intervention and, hence, avoid unsafe water distribution. In this context, a porous silicon membrane (pSiM)-based electrochemical biosensor was developed for direct and sensitive detection of LPS. pSiM, featuring arrays of nanochannels, was modified with polymyxin B (PmB), an antimicrobial peptide with strong affinity to LPS. Detection of LPS was based on measuring the changes in the diffusion through the nanochannels of an electroactive species added in solution, caused by the nanochannel blockage upon LPS binding to PmB. Results showed a limit of detection (LOD) of 1.8 ng/mL, and a linear response up to 10,000 ng/mL spiked in buffer. Selectivity of the sensor towards potential interfering species in water supplies was also assessed. Sensor performance was then evaluated in water samples from a water treatment plant (WTP) and detection of LPS well below the levels encountered in episodes of water contamination and in humidifiers was demonstrated. The same platform was also tested for bacterial detection including *Pseudomonas aeruginosa* (*P. aeruginosa*) and *Escherichia coli* (*E. coli*) spiked in water samples from a WTP. Considering its performance characteristics, this platform represents a promising screening tool to identify the presence of LPS in water supplies and provide early warning of contamination events.

Keywords: Lipopolysaccharides, endotoxins, porous silicon, label-free detection, electrochemical biosensor, bacterial contamination, polymyxin

Lipopolysaccharides (LPS), also known as endotoxins, are found in the outer cell membrane of Gram-negative bacteria and some cyanobacteria, and are constantly released during active cell growth and upon cell death[1-3]. LPS are composed of O-antigenic oligosaccharide side chains, a core polysaccharide chain, and a lipid component (Lipid A)[4, 5] (Figure S-1 in the Supporting Information). The O-antigen is highly variable, not ubiquitous and specific to the bacterial serotype. The core section of the molecule is divided into inner and outer core, the outer being further away from the bacterial surface. Lipid A is responsible for the toxic effects of the molecule [6], where the length of the acyl chain is the primary determinant of the toxicity [7].

LPS in water and water aerosols pose a potential health risk [8-11]. As an example, in 1978 in Finland, a high concentration of LPS in tap water (40 ng/mL) and in lake water (20-1,000 ng/mL) caused bath-water fever to more than 100 people that included repeated chills, fever, respiratory-tract symptoms and muscle pain [12]. Levels above 100 ng/mL in water supplies have been found to induce health symptoms (i.e. chills and fever) if employed in a humidifier [13]. Additionally, treatment plants where membrane filtration was not used resulted in high levels of LPS being found in the filtrate water. The presence of LPS is a useful indicator to evaluate the effectiveness of membrane filtration commonly used as a barrier to prevent bacterial contamination [14].

Current tests for LPS detection are based on colourimetric measurements, including the limunus amebocyte lysate (LAL) assay and various enzyme-linked immunosorbent assays (ELISAs) [15]. The LAL test relies on the clotting of horseshoe crab blood cells upon exposure to LPS, while in the various ELISAs, LPS content is measured via the activity of the enzyme used. Despite being highly sensitive, these methods are subject to numerous interferences, they are costly, time consuming and require skilled technicians, and thus are not ideal for real-time water control quality measurements.

Rapid, sensitive, portable and easy to use tools are required to provide early warnings of contamination events, allowing earlier intervention and, therefore, avoiding unsafe water distribution. In this context, biosensors have been shown for decades as powerful tools to screen for water contamination [16-18]. More specifically, electrochemical biosensors offer high sensitivity and have been shown to achieve very low limits of detection (LODs) for certain contaminants [19, 20]. Porous silicon has shown great potential as a sensing platform to detect low levels of biological contamination in water [16, 21]. In particular, porous silicon membrane (pSiM)-based electrochemical biosensors that exploit nanochannel blockage (NB) as the sensing strategy have demonstrated their potential as a simple, sensitive and rapid detection platform[16]. This sensing concept offers the possibility to tune the features of the porous

structure (morphology of the channel in terms of diameter and length) according to the size of the target analyte to optimise the sensitivity. Another important advantage is the capability to minimise matrix effects from interfering species that could be present in water based on size exclusion effects. Moreover, the high versatility of pSi offers the possibility to detect a broad range of analytes by simply modifying its morphology and chemistry according to the requirements of the final application. Here, pSiMs were modified with polymyxin B (PmB) due to its strong affinity to LPS, stability and low cost. The LPS-capturing properties of PmB combined with high-performing pSiM-based electrochemical transducers can pave the way towards powerful tools with improved sensing capabilities.

PmB is a cyclic amphiphilic cationic peptide with broad antimicrobial and antiendotoxic activity [22]. Binding of LPS to PmB is a two-step process; firstly, an electrostatic attraction between the charged parts of both molecules (the positively charged side-chain amino groups of the PmB and the negatively charged bisphosphorylated diglucosamine backbone of Lipid A), followed by hydrophobic interaction between their nonpolar regions (Figure S-1 in the Supporting Information) [23, 24]. Due to its anti-endotoxic activity, several PmB sensors have been developed over the last few years. Table 1 summarises the main PmB electrochemical sensors including the detection technique employed, detection range, LOD and final application. Ding *et al.* [25] developed a highly sensitive platform using Au electrodes modified by self-assembling a monolayer of 4,4-dithiodibutyric acid to introduce carboxyl groups on the electrode surface, followed by PmB immobilisation via carbodiimide chemistry. This platform was able to detect low LPS levels over the range from 0.2 to 0.8 ng/mL, that is particularly relevant in the biomedical field. Similarly, Zuzuarregui *et al.* [26] fabricated a PmB sensor via self-assembling of mercaptopropionic acid on a Au electrode. A wide range of LPS concentrations was tested, 10 – 100,000 ng/mL, achieving an LOD of 160 ng/mL. However, performance of the sensor in real samples was not demonstrated. LPS detection in real samples (i.e. water and food) was achieved using interdigitated Si sensors [27]. In this case, sensor performance was evaluated by spiking LPS over a concentration range from 100 ng/mL to 1,000,000, with 100 ng/mL being the lowest concentration detected. Although these sensors were able to detect LPS, either the LODs were too high to be used in water supplies or their performance was not evaluated in real samples.

Here, PmB sensors prepared with pSiMs were investigated for the sensitive quantification of LPS in water supplies. Results showed excellent sensitivity to identify the presence of LPS at the levels regularly encountered in LPS contaminated water episodes and in humidifiers. The excellent performance of the developed pSiM-based electrochemical sensors bodes well for the use in devices for simple, direct and sensitive water quality control.

Table 1. PmB electrochemical sensors for the detection of LPS.

Platform	Detection technique	Detection range (ng/mL)/ Type of LPS	LOD (ng/mL)	Application	Reference
pSiMs-modifed electrode	DPV	1 -10,000 *E. coli O1:B44* *S. typhimurium*	1.8 (*E. coli*) 2.6 (*S. typhimurium*)	Real water samples	**This work**
Au electrode	EIS	0.2 - 0.8 *E. coli O1:B44*	Not provided	Not tested	[25]
Au electrode	EIS	10 – 100,000 *E. coli ATCC35218*	160	Not tested	[26]
Interdigitated thin film Si-based sensor	EIS	100 – 1,000,000 *E. coli O1:B44*	Not provided	Samples of water and food (milk, cucumber, beef, chicken)	[27]

pSiM: porous silicon membrane

DPV: differential pulse voltammetry

EIS: electrochemical impedance spectroscopy

E. coli: Escherichia coli

S. typhimurium: Salmonella typhimurium

Experimental

Chemicals and instruments

N-type Si wafers with 0.008-0.02 Ωcm resistivity, phosphor doped, (100)-oriented were purchased from Siltronix (France). Au coated microscope slides, consisting of 150 nm of gold (Au) coating on a 10 nm chromium layer, were purchased from Telic Company (USA).

Potassium ferrocyanide ($K_4[Fe(CN)_6]$), potassium ferricyanide ($K_3[Fe(CN)_6]$), undecylenic acid, N-hydroxysuccinimide (NHS), N-(3-dimethylaminopropyl)N′-ethylcarbodiimide hydrochloride (EDC), ethanolamine (ETA), Dulbecco's phosphate buffered saline (DPBS), 2-(N-morpholino)-ethanesulfonic acid (MES), polymyxin B (PmB), lipopolysaccharides purified from *Escherichia coli* O111:B4 (L4130, purified by trichloroacetic acid extraction, with 1-10% protein impurities) and from *Salmonella enterica serotype typhimurium* (L6511, purified by phenol extraction, with < 3% protein impurities), 2-2'-(ethylenedioxy)bis(ethylamine) (EDEA), Lysogeny broth (LB) agar and silanised glass vials were purchased from Sigma-Aldrich (Australia). Hydrofluoric acid (HF) (48%, AR grade) was purchased from Scharlau (Australia). Sodium hydroxide (NaOH) (AR grade) was purchased from Merck (Australia) and NCW-1001 surfactant was purchased from Wako Pure Chemical Industries (Japan). All solutions were prepared in Milli-Q water and all reagents were used as received.

A commercial ELISA kit for LPS detection was purchased from Elabscience (E-EL-0025).

Electrochemical anodisation of silicon was performed using a Keithley source meter (Model 2425, USA).

Scanning Electron Microscopy (SEM) was employed to determine the morphological characteristics of the pSiMs, such as channel diameter and length. SEM images were obtained on a FEI QuantaTM 450 Field Emission Gun Environmental Scanning Electron Microscope.

Atomic Force Microscopy (AFM) imaging was performed using a NanoWizard III BioAFM (JPK Instruments, Berlin) with Si_3N_4 probes (SLN-10) purchased from Bruker AFM probes (Singapore).

All surface modification steps of pSiM were characterised by Fourier transform infrared spectroscopy (FT-IR) in reflectance mode using a Hyperion 1000 microscope (Bruker Optics, Germany) coupled to a liquid nitrogen cooled mercury-cadmium-tellurite detector. Spectra were analysed using Optus software (Bruker).

Dynamic light scattering (DLS) was performed to characterise the mean effective diameter of LPS using a PSS Nicomp 380 instrument (Particle Sizing System Inc., USA). 1 mg/mL of LPS solution was prepared in DPBS (sterile-filtered, without $CaCl_2$ or $MgCl_2$) and transferred to a 3 mL quartz cuvette to undertake DLS measurements at room temperature.

All LPS solutions were incubated on the biosensor surface using a temperature-controlled shaker (New Brunswick Scientific, model C 24, Australia).

All electrochemical measurements were carried out on an electrochemical analyser (Dropsens, model 8000, Spain) using a three-electrode Teflon cell containing the pSiMs on a Au substrate as the working electrode, a Ag/AgCl reference electrode and a Pt wire as counter electrode.

Preparation of the pSiM-modified electrode

The pSiM-modified electrode was prepared as described in our previous work[21], and as shown in Scheme 1. Briefly, pSi was fabricated by electrochemical anodisation of single crystal Si wafers in 5.5% aqueous HF solution (25 mL HF, 200 mL deionised water and 1 mL NCW-1001surfactant) (Scheme 1B). pSi with three nanochannel diameters was fabricated by modifying the etching current intensities and time: 11.3 mA/cm^2 for 175 s, 14.3 mA/cm^2 for 140 s and 19.8 mA/cm^2 for 100 s, respectively. The morphological characteristics of the anodised pSi structures, including channel diameter and length, were determined by analysis of the acquired SEM images for each type of structure. To obtain membranes, electrochemical anodisation was followed by the pSiMs detachment from the Si substrate by applying a series of high current pulses (electropolishing) (Scheme 1C). pSiMs, featuring arrays of nanochannels, were then transferred to Au surfaces (Scheme 1D).

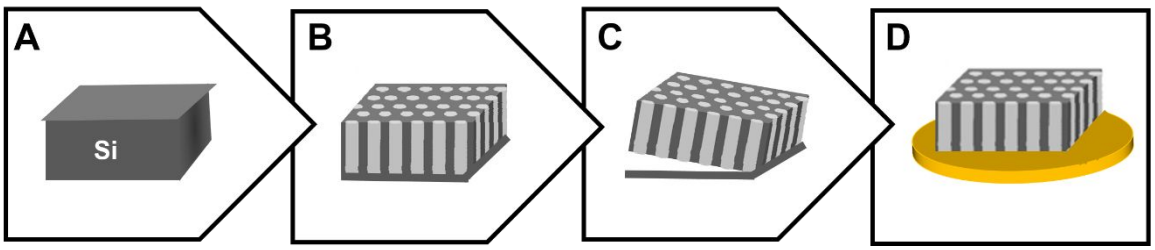

Scheme 1. Fabrication of the pSiM-modified electrode, involving the following steps: (B) electrochemical anodisation of Si, (C) pSiM detachment by electropolishing and (D) transfer to a Au electrode.

Modification of the pSiM

Surface modification steps for the pSiM are shown in Scheme 2. Freshly etched pSiMs were hydrosilylated with neat undecylenic acid at 150 °C for 12 h under an argon gas stream to introduce carboxyl groups. The carboxyl-terminated surface was then rinsed with copious amounts of ethanol, followed by activation with 5 mM 1-(3-dimethylaminopropyl)-3-ethylcarbodiimide (EDC) and 5 mM N-hydroxysuccinimide (NHS) in 0.1 M MES buffer (pH 5) at room temperature for 30 min. Thereafter, NHS ester groups were reacted with 100 µg/mL polymyxin B (PmB) in DPBS for 2 h at room temperature in a shaker, followed by overnight incubation at 4 °C. The remaining ester groups were deactivated with 0.1 M ethanolamine (ETA) in DPBS for 45 min. After each step, pSi was copiously rinsed with DPBS. A negative control pSiM was prepared under similar conditions incubating 2-2'-(ethylenedioxy)bis(ethylamine) (EDEA) instead of PmB after EDC/NHS activation.

Each surface modification step of pSiM was confirmed by FT-IR in reflectance mode, by acquiring an average of 64 scans, with a resolution of 4 cm^{-1}, and over the range of 650–4000 cm^{-1}. Background spectra were performed using an Au coated glass slide.

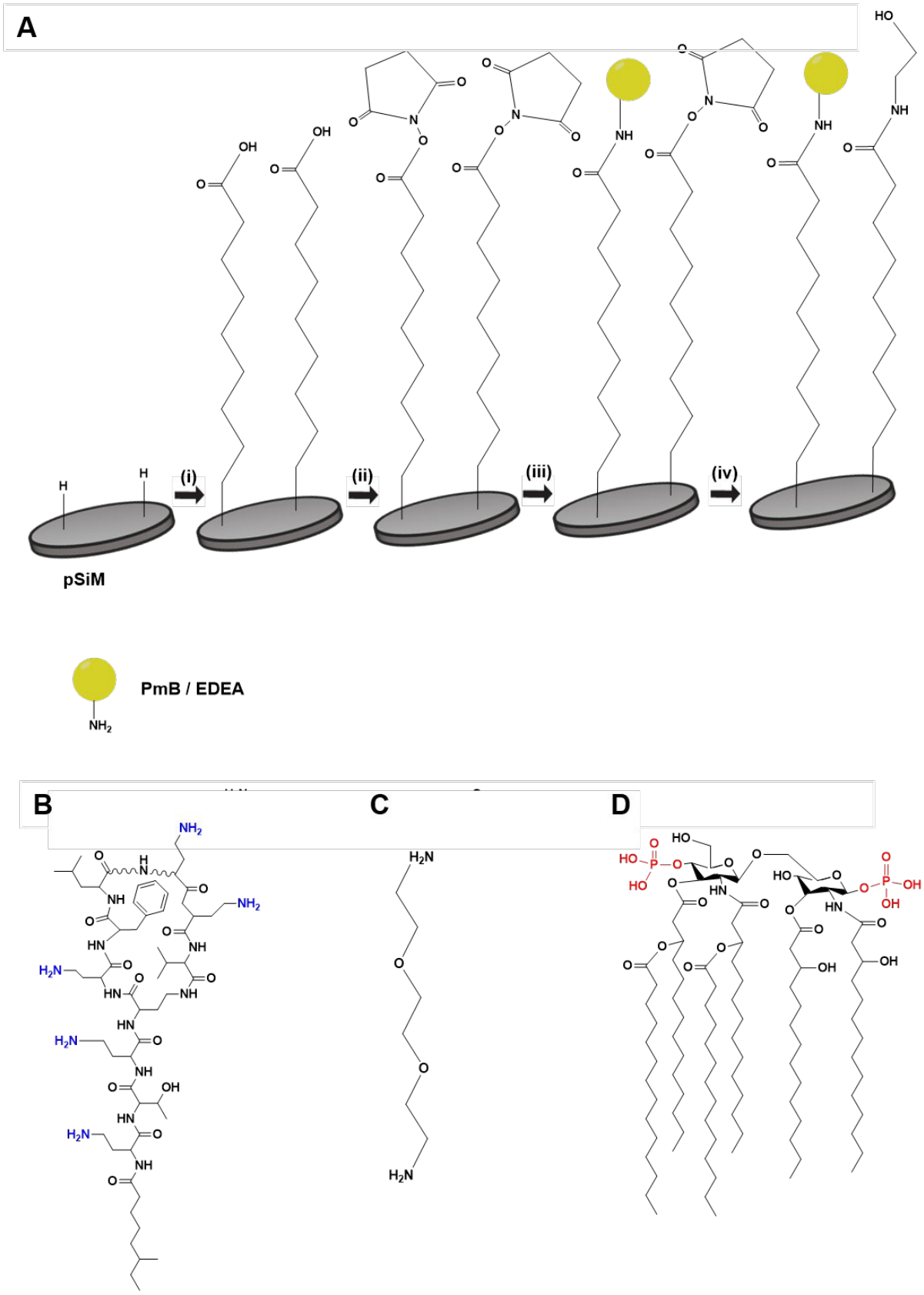

Scheme 2. (A) Surface modification steps of the pSiMs including (i) thermal hydrosilylation, (ii) EDC/NHS activation, (iii) PmB or EDEA immobilisation, and (iv) quenching with ETA. Structure of (B) PmB, (C) EDEA and (D) Lipid A of LPS. Binding of LPS to PmB starts via

electrostatic attraction between the positively charged amino groups of PmB (in blue in (B)) and the negatively charged phosphate groups of Lipid A (red in (D)) [23].

Electrochemical detection of LPS

LPS detection in buffer

Solutions of LPS from *E. coli O111:B4* ranging from 1 to 10,000 ng/mL were prepared in DPBS buffer and incubated on the pSiM-based sensor surface for 1 h at 37 °C in an orbital shaker at 60 rpm. LPS solutions were prepared according to the supplier instructions using silanised vials to avoid adsorption to the walls, followed by 5 min sonication. After each incubation, electrodes were thoroughly washed with DPBS. DPV was used as the electrochemical technique to measure changes in the diffusion through the nanochannels of the added redox probe, caused by LPS binding to the immobilised PmB. DPV measurements prior and after LPS incubation were carried out in a solution of 2 mM $K_4[Fe(CN)_6]$ and 2 mM $K_3[Fe(CN)_6]$ in DPBS. pSiM-based sensors featuring three different nanochannel diameters were tested, functionalised with either PmB or EDEA (control). For comparison purposes, current intensity values were normalised as follows: $\Delta I = (I_0 - I)/I_0$, where ΔI is the normalised current change, and I_0 and I are the current intensity values measured prior and after LPS incubation.

The ability to detect other bacterial LPS such as those released by *Salmonella typhimurium* (*S. typhimurium*) was investigated using the same procedure described above. In those experiments, the nanochannel diameter pSiM providing the highest sensitivity towards LPS from *E. coli O111:B4* was employed, modified with PmB or EDEA.

PmB-modified pSiM-based sensors with the optimum channel diameter were used to test their selectivity by measuring the electrochemical response towards various interfering species, including LPS components (i.e. glucose), 10,000 pfu/mL MS2 bacteriophage and 10,000 plaque forming unit (pfu)/mL murine norovirus (MNV). Each solution was prepared in DPBS buffer and incubated on the sensor surface for 1 h at 37 °C. After each incubation step the sensor was washed with DPBS buffer. The DPV response was measured prior and after incubation.

All voltammograms were obtained by scanning the potential from -0.3 V to 0.8 V and each assay was performed in triplicate.

LPS detection in WTP spiked water samples

Water samples were collected from the Happy Valley WTP (Happy Valley, South Australia). The samples were first analysed using a commercial ELISA kit, and those free of LPS were spiked with LPS from *E. coli O111:B4*, in a concentration range from 1 to 10,000 ng/mL, to test the performance of the sensors in real water samples. The LPS spiked WTP water samples were incubated on the optimised pSiM-based sensors (modified with either PmB or EDEA) in an orbital shaker for 1 h at 37 °C and 60 rpm. After each incubation step, electrodes were washed with DPBS. DPV measurements were carried out before and after incubation. Each assay was performed in triplicate.

Bacterial detection

The possibility to detect LPS forming the outer membrane of Gram-negative bacteria was attempted using pSiM-based sensors with the largest channel diameter. WTP water samples spiked with *P. aeruginosa* (ATCC27853) and *E. coli* (ATCC2592) were incubated on pSiM-based sensors modified with either PmB or EDEA. Bacteria were cultured by plating them on agar plates followed by an overnight incubation at 37 °C. Thereafter, single bacterial colonies were isolated and incubated for 24 h at 37 °C in LB broth medium. Bacteria were removed from the media by centrifugation at 8,000g for 10 min and suspended in DPBS. This washing procedure was repeated three times. The bacterial concentration was then measured by means of turbidity, measuring the optical density at a wavelength of 600 nm. Finally, bacterial dilutions from 1 to 10^5 colony forming unit (cfu)/mL were prepared in WTP samples and incubated for 1 h on the surface of the pSiM-based sensors. After each incubation step, sensors were washed with DPBS. DPV measurements were performed prior and after incubation. Each assay was performed in triplicate. The presence of *P. aeruginosa* and *E. coli* on the surface of the PmB-modified pSiM was examined by means of AFM with Si_3N_4 probes, with frequencies of 50–80 kHz and spring constant of 0.35–0.7 N/m, in liquid (DPBS) at room temperature. pSiMs with the largest channel diameter were incubated for 1 h with WTP water samples unspiked (used as a control), and spiked with 10^4 cfu/mL *P. aeruginosa* and 10^4 cfu/mL *E. coli*. Membrane was carefully and thoroughly washed with DPBS prior imaging.

Results

Morphological characterisation of the pSiM

pSiM-based sensors with three nanochannel diameters were fabricated to investigate the effect of the nanochannel diameter on the sensitivity of the sensor. Scanning electron microscopy (SEM) was used to characterise the nanochannel diameter and thickness of each pSiM. Figure 1 shows the top and cross-sectional SEM images of the three membranes with average nanochannel diameters of 40 ± 15 nm, 57 ± 17 nm and 85 ± 23 nm, and an estimated total thickness of ~ 4.5 μm.

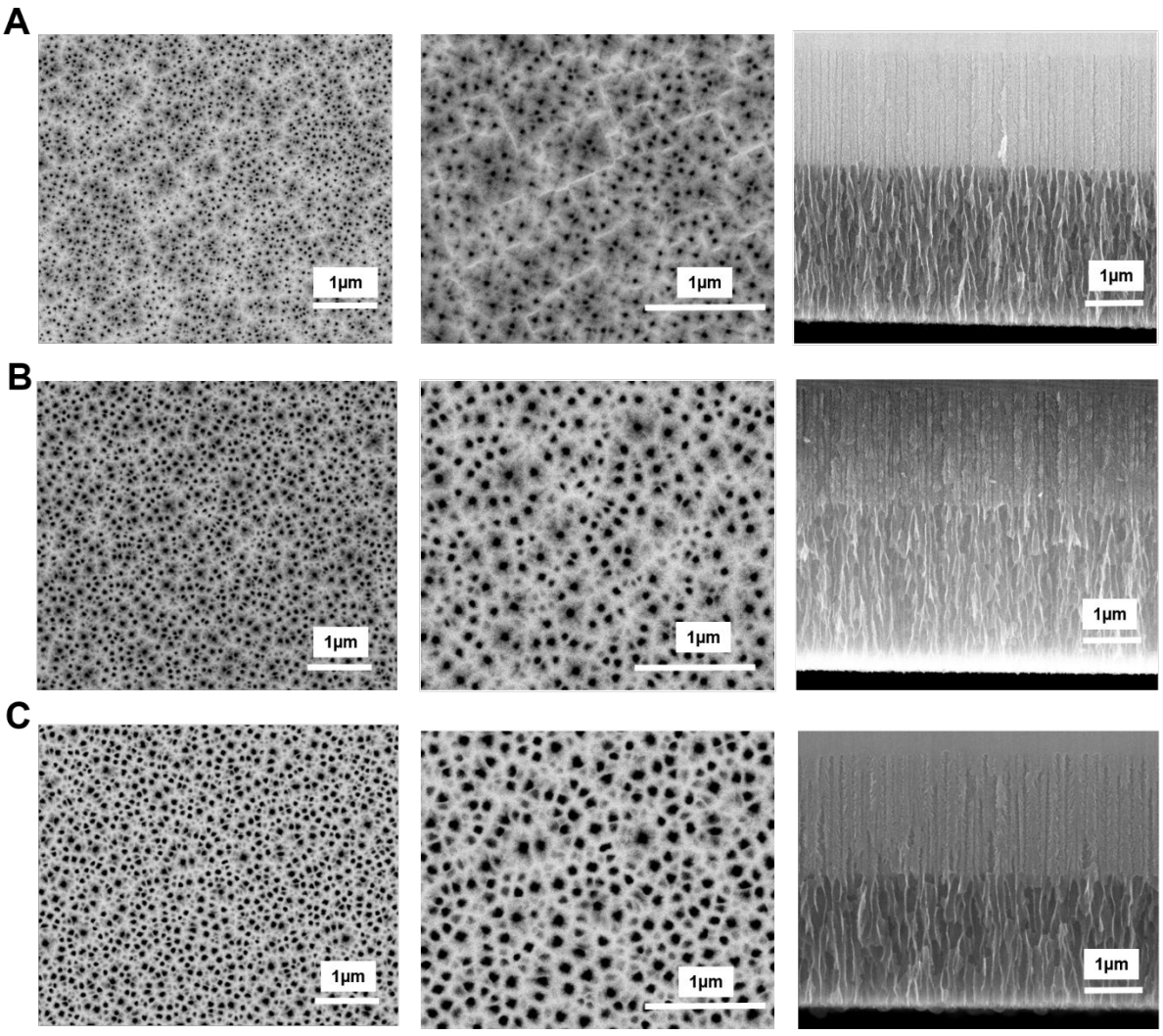

Figure 1. SEM micrographs of the top and cross-sectional views of the membranes etched at the following current intensities: (A) 11.3 mA/cm^2, (B) 14.3 mA/cm^2 and (C) 19.8 mA/cm^2.

FT-IR characterisation of the pSiM

All surface modification steps described in section 2.3 were characterised by FT-IR in reflectance mode as shown in (Figure 2, and Figure S-2 in the Supporting Information).

Spectrum A in Figure 2 (also in Figure S-2) shows peaks that correspond to the stretching vibrational mode of the vC=O of the carboxylic acid (1714 cm^{-1}) and vCH_2 of the aliphatic C-H (2890 and 2940 cm^{-1}), confirming the modification of the Si-H with undecylenic acid. Carbodiimide activation of the carboxyl groups was confirmed by the triplet bands at 1740, 1785 and 1815 cm^{-1} in Figure 2B (also in Figure S-2B), followed by PmB (Figure 2C) and EDEA (Figure S-2C) coupling. The appearance of two broad bands at around 1650 and 1550 cm^{-1}, corresponding to the C=O stretch and vN-H bend, respectively, demonstrates the successful immobilisation of PmB and EDEA. Note that the two broad peaks at around 3400 cm^{-1} and 2400 cm^{-1} in all spectra are due to the interference of the IR light with the pSi film [28].

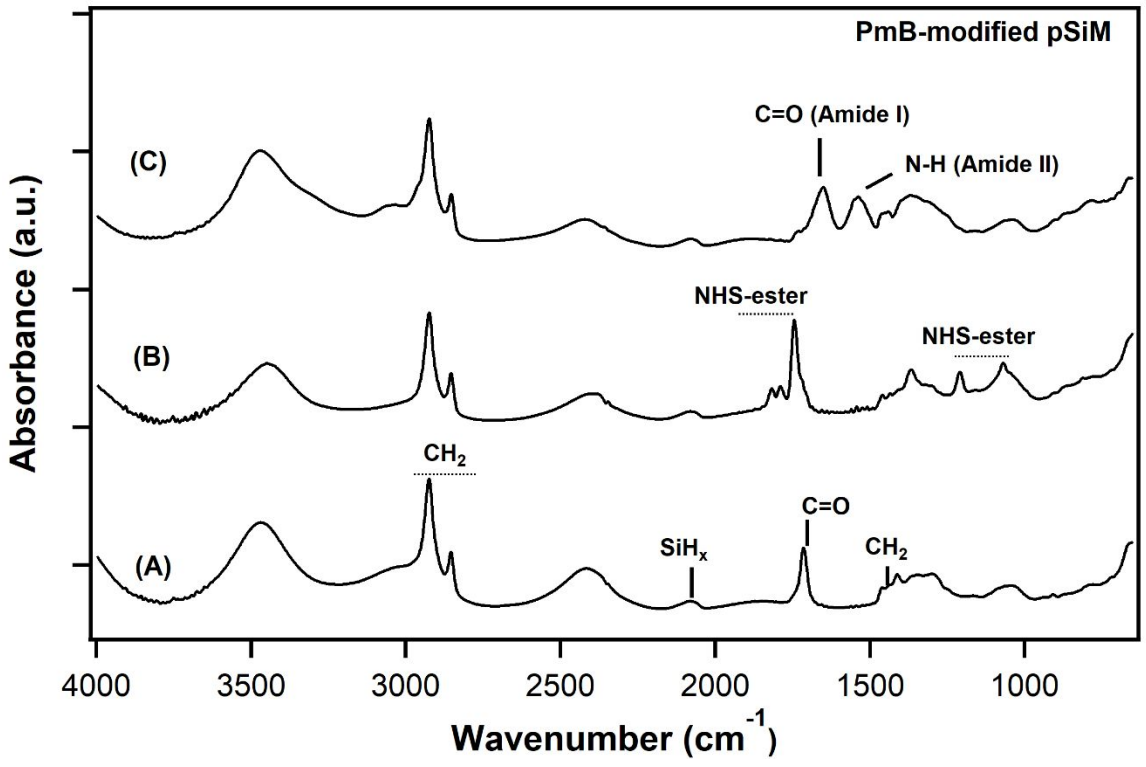

Figure 2. Reflectance mode FT-IR spectra of the pSiM after (A) thermal hydrosilylation, (B) EDC/NHS activation and (C) PmB immobilisation.

Electrochemical LPS detection in buffer

The sensing principle of LPS detection is based on quantifying the changes in the diffusion of the redox probe added in solution, as a result of the LPS binding to the immobilised PmB[21, 29, 30] and blocking the channel. These changes are determined by measuring the current intensity produced by the oxidation of the redox probe on the Au electrode. LPS from *E. coli O111:B4* solutions from 1 – 10,000 ng/mL were prepared in DPBS. The average hydrodynamic diameter of LPS from *E. coli O111:B4* in DPBS was found to be 12.0 ± 5.7 nm (Figure S-3 in the Supporting Information), confirming that LPS diffusion through the nanochannels and binding to immobilised PmB is possible even for the pSiM-based sensors featuring the smallest nanochannel diameter (40 nm). LPS solutions were incubated on the pSiM-based sensor surface, modified either with PmB or EDEA (control), for 1 h. DPV measurements were performed before and after each LPS incubation to determine binding of LPS to the immobilised PmB. Figure 3 shows DPV traces for pSiM-based sensors featuring 40 nm, 57 nm and 85 nm channel diameter. The results clearly show a dramatic decrease in current intensity for all sensors modified with PmB over a wide range of concentrations (from 1 – 10,000 ng/mL). Changes for the EDEA-modified sensor (control) were insignificant (Figure 3B, D, F), confirming the affinity of LPS to the immobilised PmB, and negligible non-specific interactions.

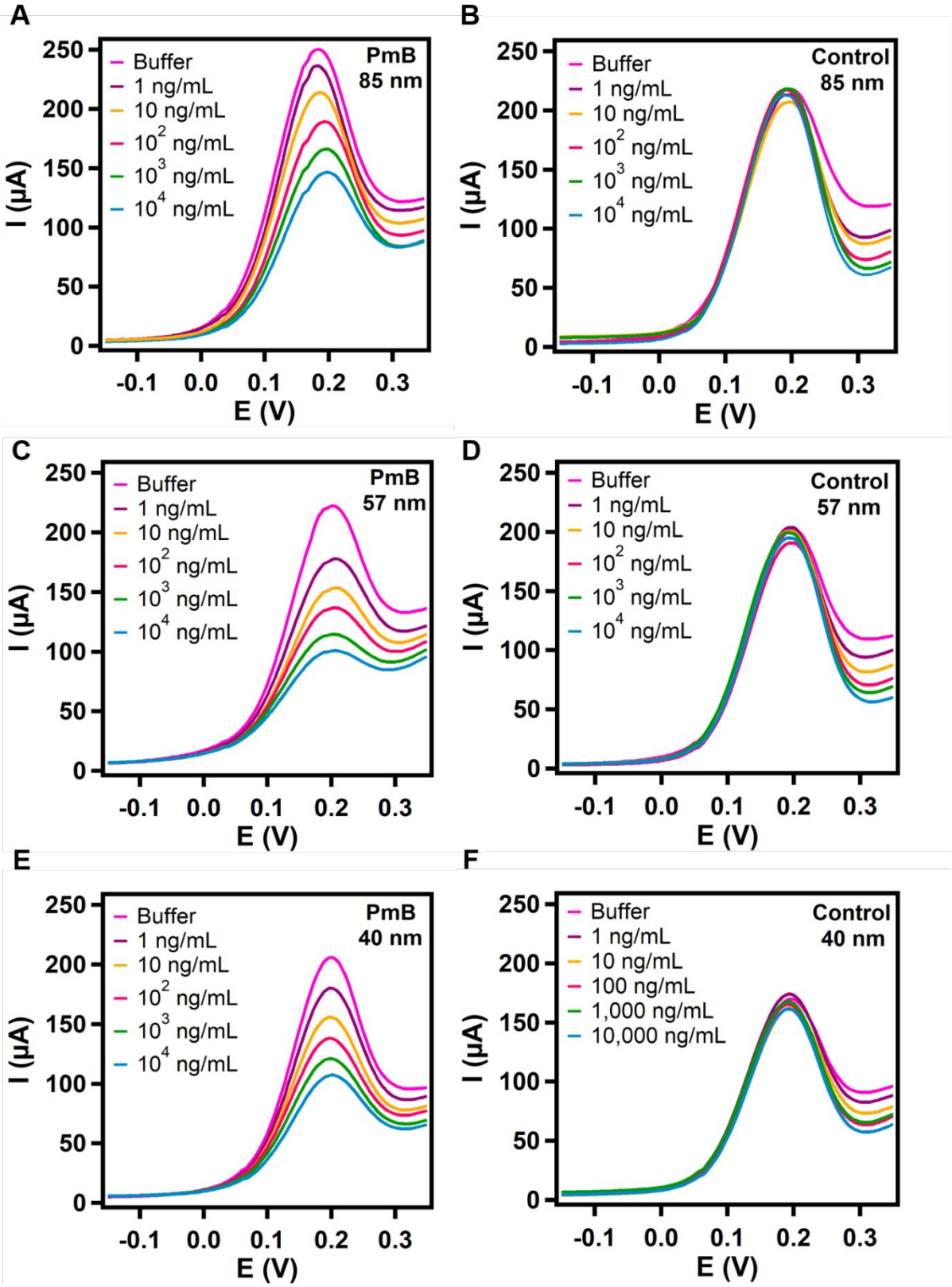

Figure 3. Differential pulse voltammograms for increasing concentrations of LPS from *E. coli* in buffer for: (A, C, E) PmB- and (B, D, F) EDEA (control)-modified pSiM-based sensors with 40 nm, 57 nm and 85 nm channel diameter, respectively.

Dose response curves for all sensors functionalised with either PmB or EDEA are shown in Figure 4A. Since the sensing mechanism relies on changes in the diffusion of the redox probe through the nanochannels, the effect of the pSiM channel diameter on the PmB-modified sensor performance was investigated by comparing the sensitivity and LOD achieved by the sensors featuring 40 nm, 57 nm and 85 nm nanochannel diameters, respectively. The sensitivity of the PmB sensors, determined by the slope of the linear fitting curve, increased as follows depending on the channel diameter: 40 nm < 85 nm < 57 nm (Figure 4B). Based on these results, the LOD values, calculated using the equation $3S_a/b$, where S_a is the standard deviation of the y-axis and b is the slope [31], were found to be 1.8 ± 0.11 ng/mL, 2.1± 0.28 ng/mL and 2.9 ± 0.20 ng/mL for the pSiM-based sensors with 57 nm, 40 nm and 85 nm channel diameters, respectively.

A

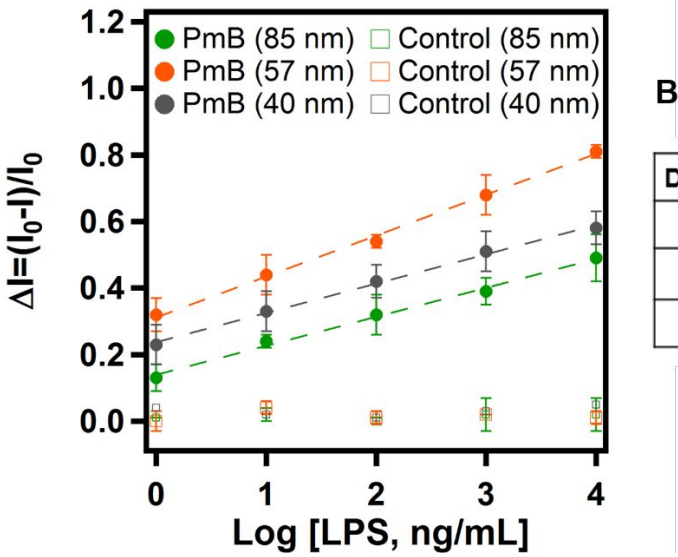

B

D (nm)	Regression curve	R^2
40	ΔI = 0.091log[LPS] + 0.232	0.994
57	ΔI = 0.122log[LPS] + 0.314	0.997
85	ΔI = 0.087log[LPS] + 0.141	0.994

Figure 4. (A) Dose repose curves for pSiM-based sensors with 40 nm, 57 nm and 85 nm channel diameter functionalised either with PmB (circle symbols) and EDEA (control) (square symbols). Each curve corresponds to the average of the response obtained by three sensors. (B) Dose response curve parameters for PmB sensors derived from the linear fitting, with D being the channel diameter of the pSiM.

The selectivity of the PmB-modified pSiM-based sensors against possible interfering components in water samples, including LPS host-derived species, such as sugars, and viruses, was investigated. PmB sensors were incubated with 50 µg/mL glucose, 10,000 pfu/mL MS2 bacteriophage and 10,000 pfu/mL MNV, without showing a significant current

response (Figure 5). Indeed, addition of these species produced changes in current that were negligible even for concentrations 50,000 times higher (i.e. glucose) than the LPS concentration used, demonstrating the high selectivity of the developed PmB biosensor.

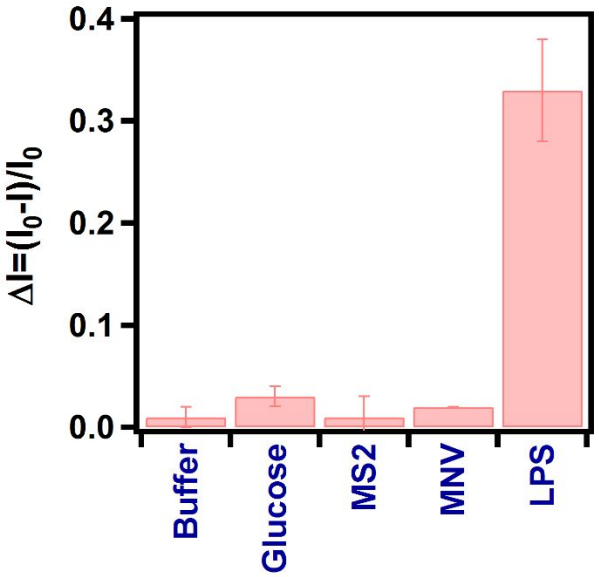

Figure 5. Selectivity of the PmB modified pSiM-based sensor with 57 nm channel diameter upon incubation of various interfering species in buffer. [Glucose] = 50 µg/mL, [MS2] = 10,000 pfu/mL, [MNV] = 10,000 pfu/mL and [LPS]= 1 ng/mL. Incubation time= 1 h.

Furthermore, the ability to detect LPS produced by other bacteria such as *S. typhimurium* was also tested in buffer (Figure 6). For purpose of comparison, the electrochemical response as a function of the concentration of LPS from *E. coli* (from 1 to 10,000 ng/mL) was also plotted. Using the PmB-modified pSiM-based sensor we successfully detected LPS from *S. typhimurium.* The PmB sensor performs differently when exposed to LPS from *E. coli* or *S. typhimurium*, the latter providing a linear response in a narrower concentration range. When comparing the PmB sensor performance for both bacterial LPS, better sensitivity was observed for *S. typhimurium* than *E. coli*, judging from the slope of the linear part of the curve, while the LOD was found to be lower for *E. coli* (1.8 ng/mL, calculated using the equation $3S_a/b$) than *S. typhimurium* (42 ng/mL, calculated as the concentration corresponding to the 10% of the PmB binding response fitted to a four-parameter logistic regression curve). This could be attributed to the structural differences in the Lipid A structure of both bacterial LPS molecules that affect the affinity of the interaction with the PmB [23, 32].

A

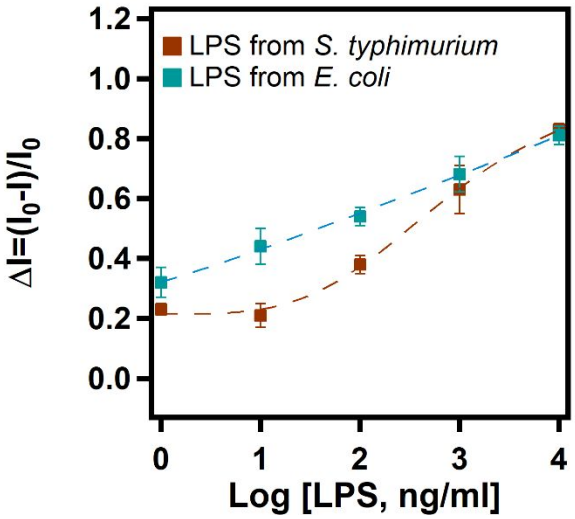

B

LPS	Regression curves	R^2
S. typhimurium	$\Delta I = 1.028 - \frac{43.2712}{53.2175 + (\log[LPS])^{3.675}}$	0.990
E. coli	$\Delta I = 0.122 \log[LPS] + 0.314$	0.997

Figure 6. (A) Dose response curves from LPS from different bacterial sources, including *S. typhimurium* and *E. coli* in DPBS, using the PmB-modified pSiM-based sensor with 57 nm channel diameter and (B) the corresponding regression curves.

Having successfully demonstrated the ability to detect LPS in buffer, the performance of the PmB-modified pSiM-based sensor with 57 nm channel diameter (which gave the best performance in the previous experiments) in real water samples was studied. First, a commercial ELISA kit was employed to test for the presence of LPS in water samples collected from the Happy Valley WTP in South Australia. Once confirmed via ELISA that they were free of LPS (Figure S-4 and Table S-1 in the Supporting Information), matrix effects were studied by incubating WTP water samples on the PmB sensor several times during 1 h. Results (Figure S-5 in the Supporting Information) showed insignificant changes (average standard deviation of ± 0.9%) upon incubation with WTP water samples, the measured current intensity being unaffected by any potentially interfering species. Next, LPS-free water samples were spiked with LPS from *E. coli* in a concentration range from 1 to 10,000 ng/mL to test the performance of PmB sensors exposed to WTP samples.

Figure 7 shows the dose response curves of LPS from *E. coli* spiked in WTP water samples using pSiM-based sensors with 57 nm channel diameter. Curves in DPBS were also added to allow comparison between the sensor performance in real (WTP samples) and ideal (buffer) conditions. Changes in the normalised current intensity increased linearly with increasing concentrations of LPS spiked in WTP water, with a regression curve of (ΔI = 0.119log[LPS] + 0.045) and with excellent linearity (R^2 = 0.998). The PmB sensor response was unaffected by matrix effects from the water samples used, as indicated by the small slope deviation between both curves (< 3%), and by the achieved LOD (1.7 ng/mL), which is similar to that obtained in buffer. Interestingly, these LOD values are in the range of concentrations encountered during episodes of water contamination [12] or in water tanks used in humidifiers [13]. Hence these results suggest that this biosensor could be employed to monitor the efficacy of membrane filtration to prevent bacterial contamination [14]. This is particularly important for water management plans incorporating the reuse of reclaimed water to address the increasing demand of water, and where there is likely to be a considerable LPS activity [33, 34].

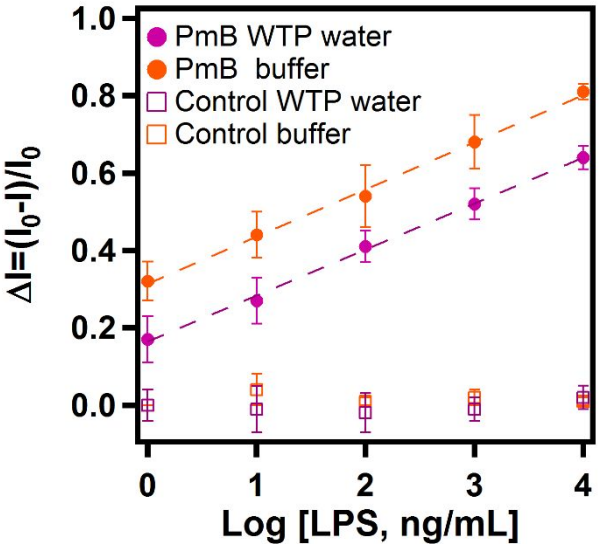

Figure 7. Dose response curves of LPS from *E. coli* spiked in WTP water samples (purple) and DPBS (orange), using PmB-modified (circle symbols) and EDEA-modified (square symbols) pSiM-based sensors with 57 nm channel diameter.

Bacterial detection

The possibility to detect LPS associated Gram-negative bacteria, including *Pseudomonas aeruginosa* (*P. aeruginosa)* and *E. coli*, was attempted using PmB-modified pSiM-based

sensors. Both types of bacteria were spiked in LPS-free WTP water samples and incubated on the pSiM-based sensor featuring 85 nm nanochannel diameter. Although this channel diameter is not large enough for bacteria (1 to 2 μm sized) to penetrate inside of the channels, spiking bacteria in water may cause bacterial cell damage due to a difference in the osmotic pressure [35]. As a consequence, bacteria might be lysed, splitting into fragments, but also may release LPS from their cell membrane [36]. To allow the small bacterial fragments entering the channels, the sensor prepared with the pSiM showing the nanochannels with the largest diameter was employed. WTP water samples spiked with bacteria in the concentration range from 1 cfu/mL to 10,000 cfu/mL, were incubated on the PmB- and EDEA-modified pSiM-based sensor surface with 85 nm channel diameter (cfu: colony forming unit). Electrochemical measurements before and after incubation were performed by means of DPV. Results in Figure 8 show significant current changes for the PmB-modified-pSiM-based sensors after incubation with both bacteria, while no changes were detected for the EDEA-modified sensors used as control. The PmB biosensors were able to detect as low as 1 cfu/mL for both bacteria. When comparing the PmB biosensor performance towards the detection of both types of bacteria, a 56% higher sensitivity for *P. aeruginosa* (0.095 mL/cfu) than for *E. coli* (0.042 mL/cfu) was observed, which is in accordance with previous reports that confirm the higher affinity of PmB for *P. aeruginosa* compared to *E. coli* [23]. Based on the results for bacterial sensing, the measured changes in the oxidation current of the redox probe added in solution, could be caused by the changes in its diffusion through the nanochannels resulting from the pSiM surface blockage upon bacteria or bacterial fragments binding, pSiM channel blockage as a result of released LPS or small bacterial fragments binding (if they are < 85 nm), or a combination of both. To support one of these hypotheses, AFM analysis of the PmB-functionalised pSiM surface was performed in liquid environment [37, 38], after thorough and careful wash of the membrane, to investigate the presence of bacteria on the surface. AFM images (Figure S-6 in the Supporting Information) obtained for pSiMs incubated with both *P. aeruginosa* and *E. coli* bacteria did not show any signs of attachment of bacteria or bacterial fragments. Hence, the changes observed upon bacteria incubation using the PmB sensor were probably caused by binding of the LPS released by these bacteria, upon spiking in water, to the immobilised PmB.

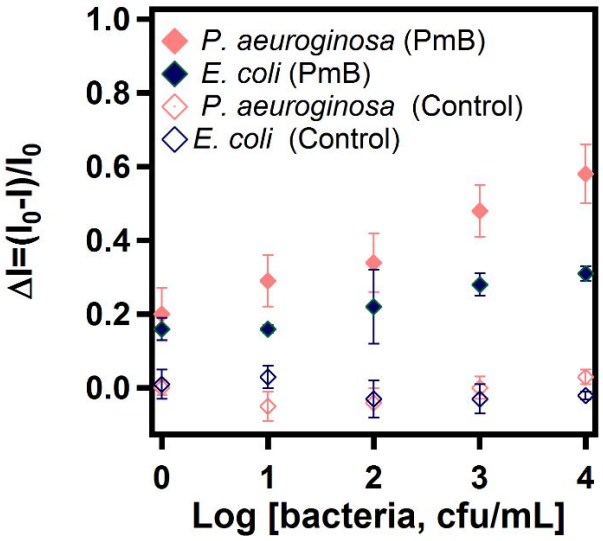

Figure 8. Detection of bacterial LPS after incubation of *P. aeruginosa* (pink) and *E. coli* (dark blue) spiked in WTP water samples on PmB- (filled symbols) and EDEA- (control) (unfilled symbols) modified pSiM-based sensors featuring 85 nm diameter channels.

Conclusions

Low levels of LPS were detected using PmB-modified pSiM-based sensors in a label-free manner and about 2 to 3 times faster than the current methods [39, 40]. The sensor showed a LOD of 1.8 ng/mL LPS in buffer, as well as the ability to detect different bacterial LPS such as those released by *E. coli* and *S. typhimurium*. The selectivity of this platform towards some interfering species that are likely to coexist in water supplies was also evaluated and shown to be unaffected. Furthermore, the feasibility to detect LPS in spiked water samples from a WTP was demonstrated by achieving LODs at the levels encountered in real-world water applications such as episodes of water contamination and in humidifiers. Additionally, indirect detection of Gram-negative bacteria, *P. aeruginosa* and *E. coli*, via quantification of their released LPS, was also achieved, at the level of 1 cfu/mL of both bacteria. The excellent analytical performance of this platform highlights its potential to be used as a control device to assess the effectiveness of the barriers employed to prevent bacterial contamination, as well as, as a routine screening tool for water quality control.

Supporting Information

The Supporting Information is available free of charge on the ACS Publications website. The file includes figures of LPS structure, FT-IR spectra for each functionalisation step of the control sensor modified with EDEA, size distribution of LPS from *E. coli O111:B4* in buffer,

ELISA results for the LPS analysis of water samples, electrochemical response of PmB sensors upon consecutive incubations of WTP water samples, and AFM images of PmB- and EDEA-modified pSiM after exposure to *P. aeruginosa* and *E. coli* spiked in WTP water samples.

Acknowledgment

The authors are grateful for financial support from the Australian Research Council's Linkage Project Scheme (LP130100032), and also acknowledge the National Centre of Excellence in Desalination Australia (NCEDA) for providing top-up scholarship for NR and the University of South Australia for an International President's scholarship for NR. This work was performed in part at the Melbourne Centre for Nanofabrication (MCN) in the Victorian Node of the Australian National Fabrication Facility (ANFF).

References

1. Madigan, M.; Martinko, J.; Parker, J., Brock Biology of Microorganisms. Southern Illinois University Carbondale. Prentice Hall International, Inc: 2000.
2. Keleti, G.; Sykora, J. L.; Lippy, E. C.; Shapiro, M. A., Composition and biological properties of lipopolysaccharides isolated from Schizothrix calcicola (Ag.) Gomont (Cyanobacteria). *Applied and Environmental Microbiology* **1979,** *38* (3), 471-477.
3. Brooks, J. P.; Tanner, B. D.; Gerba, C. P.; Pepper, I. L., The measurement of aerosolized endotoxin from land application of Class B biosolids in Southeast Arizona. *Canadian Journal of Microbiology* **2006,** *52* (2), 150-156.
4. Qiao, S.; Luo, Q.; Zhao, Y.; Zhang, X. C.; Huang, Y., Structural basis for lipopolysaccharide insertion in the bacterial outer membrane. *Nature* **2014,** *511* (7507), 108-111.
5. Sigma-Aldrich Glycobiology Analysis Manual 2nd Edition. http://www.sigmaaldrich.com/life-science/proteomics/post-translational-analysis/glycosylation/glycoprotein-analysis-manual.html.
6. Morrison, D. C.; Danner, R. L.; Dinarello, C. A.; Munford, R. S.; Natanson, C.; Pollack, M.; Spitzer, J. J.; Ulevitch, R. J.; Vogel, S. N.; McSweegan, E., Bacterial endotoxins and pathogenesis of Gram-negative infections: current status and future direction. *Journal of Endotoxin Research* **1994,** *1* (2), 71-83.
7. Erridge, C.; Bennett-Guerrero, E.; Poxton, I. R., Structure and function of lipopolysaccharides. *Microbes and Infection* **2002,** *4* (8), 837-851.
8. Anderson, K.; McSharry, C. P.; Clark, C.; Clark, C. J.; Barclay, G. R.; Morris, G. P., Sump bay fever: inhalational fever associated with a biologically contaminated water aerosol. *Occupational and Environmental Medicine* **1996,** *53* (2), 106-111.
9. Anderson, W. B.; Slawson, R. M.; Mayfield, C. I., Review / SynthèseA review of drinking-water-associated endotoxin, including potential routes of human exposure. *Canadian Journal of Microbiology* **2002,** *48* (7), 567-587.
10. Lippy, E. C.; Erb, J., Gastrointestinal Illness at Sewickley, Pa. *Journal (American Water Works Association)* **1976,** *68* (11), 606-610.
11. Herbert, A.; Carvalheiro, M.; Rubenowitz, E.; Bake, B.; Rylander, R., Reduction of alveolar-capillary diffusion after inhalation of endotoxin in normal subjects. *Chest* **1992,** *102* (4), 1095-1098.
12. Muittari, A.; Rylander, R.; Salkinoja-Salonen, M., Endotoxin and bath-water fever. *The Lancet* **1980**, DOI: 10.1016/S0140-6736(80)92965-7
13. Anderson, W. B.; George Dixon, D.; Mayfield, C. I., Estimation of endotoxin inhalation from shower and humidifier exposure reveals potential risk to human health. *Journal of Water and Health* **2007,** *5* (4), 553-572.
14. O'Toole, J.; Sinclair, M.; Jeavons, T.; Leder, K., Alternative water sources and endotoxin. *Water Science and Technology* **2008,** *58* (3), 603-607.
15. Das, A. P.; Kumar, P. S.; Swain, S., Recent advances in biosensor based endotoxin detection. *Biosensors and Bioelectronics* **2014,** *51*, 62-75.
16. Reta, N.; Saint, C. P.; Michelmore, A.; Prieto-Simon, B.; Voelcker, N. H., Nanostructured Electrochemical Biosensors for Label-Free Detection of Water- and Food-Borne Pathogens. *ACS Applied Materials & Interfaces* **2018,** *10* (7), 6055-6072.
17. Campas, M.; Garibo, D.; Prieto-Simon, B., Novel nanobiotechnological concepts in electrochemical biosensors for the analysis of toxins. *Analyst* **2012,** *137* (5), 1055-1067.
18. Rodriguez-Mozaz, S.; Lopez de Alda, M. J.; Barceló, D., Biosensors as useful tools for environmental analysis and monitoring. *Analytical and Bioanalytical Chemistry* **2006,** *386* (4), 1025-1041.
19. Grieshaber, D.; MacKenzie, R.; Vörös, J.; Reimhult, E., Electrochemical Biosensors - Sensor Principles and Architectures. *Sensors* **2008,** *8* (3), 1400-1458.
20. Bakker, E., Electrochemical Sensors. *Analytical Chemistry* **2004,** *76* (12), 3285-3298.

21. Reta, N.; Michelmore, A.; Saint, C.; Prieto-Simón, B.; Voelcker, N. H., Porous silicon membrane-modified electrodes for label-free voltammetric detection of MS2 bacteriophage. *Biosensors and Bioelectronics* **2016,** *80*, 47-53.
22. Danner, R. L.; Joiner, K. A.; Rubin, M.; Patterson, W. H.; Johnson, N.; Ayers, K. M.; Parrillo, J. E., Purification, toxicity, and antiendotoxin activity of polymyxin B nonapeptide. *Antimicrobial Agents and Chemotherapy* **1989,** *33* (9), 1428-1434.
23. Vaara, M.; Viljanen, P., Binding of polymyxin B nonapeptide to gram-negative bacteria. *Antimicrobial Agents and Chemotherapy* **1985,** *27* (4), 548-554.
24. Ronco, C.; Klein, D. J., Polymyxin B hemoperfusion: a mechanistic perspective. *Critical Care* **2014,** *18* (3), 309 , DOI: 10.1186/cc13912
25. Ding, S.-J.; Chang, B.-W.; Wu, C.-C.; Chen, C.-J.; Chang, H.-C., A new method for detection of endotoxin on polymyxin B-immobilized gold electrodes. *Electrochemistry Communications* **2007,** *9* (5), 1206-1211.
26. Zuzuarregui, A.; Morant-Minana, M. C.; Perez-Lorenzo, E.; Martinez de Tejada, G.; Arana, S.; Mujika, M., Implementation and Characterization of a Fully Miniaturized Biosensor for Endotoxin Detection Based on Electrochemical Techniques. *Sensors Journal, IEEE* **2014,** *14* (1), 270-277.
27. Abdul Rahman, M. S.; Mukhopadhyay, S. C.; Yu, P.-L.; Goicoechea, J.; Matias, I. R.; Gooneratne, C. P.; Kosel, J., Detection of bacterial endotoxin in food: New planar interdigital sensors based approach. *Journal of Food Engineering* **2013,** *114* (3), 346-360.
28. Lin, V. S.-Y.; Motesharei, K.; Dancil, K.-P. S.; Sailor, M. J.; Ghadiri, M. R., A Porous Silicon-Based Optical Interferometric Biosensor. *Science* **1997,** *278* (5339), 840-843.
29. de la Escosura-Muñiz, A.; Merkoçi, A., Label-free voltammetric immunosensor using a nanoporous membrane based platform. *Electrochemistry Communications* **2010,** *12* (6), 859-863.
30. Escosura-Muñiz, A. d. l.; Espinoza-Castañeda, M.; Hasegawa, M.; Philippe, L.; Merkoçi, A., Nanoparticles-based nanochannels assembled on a plastic flexible substrate for label-free immunosensing. *Nano Research* **2015,** *8* (4), 1180-1188.
31. Ziegel, E. R., Statistics and Chemometrics for Analytical Chemistry. *Technometrics* **2004,** *46* (4), 498-499.
32. Netea, M. G.; Kullberg, B. J.; Joosten, L. A. B.; Sprong, T.; Verschueren, I.; Boerman, O. C.; Amiot, F.; van den Berg, W. B.; Van der Meer, J. W. M., Lethal Escherichia coli and Salmonella typhimurium endotoxemia is mediated through different pathways. *European Journal of Immunology* **2001,** *31* (9), 2529-2538.
33. Huang, H.; Wu, Q.-Y.; Yang, Y.; Hu, H.-Y., Effect of chlorination on endotoxin activities in secondary sewage effluent and typical Gram-negative bacteria. *Water Research* **2011,** *45* (16), 4751-4757.
34. Guizani, M.; Dhahbi, M.; Funamizu, N., Assessment of endotoxin activity in wastewater treatment plants. *Journal of Environmental Monitoring* **2009,** *11* (7), 1421-1427.
35. Altendorf, K.; Booth, I.; Gralla, J.; Greie, J.; Rosenthal, A.; Wood, J., Osmotic Stress. *EcoSal Plus* **2009**.
36. Kadis, S.; Weinbaum, G.; Ajl, S. J., *Bacterial Endotoxins: A Comprehensive Treatise*. Elsevier: 1971.
37. Bolshakova, A. V.; Kiselyova, O. I.; Filonov, A. S.; Frolova, O. Y.; Lyubchenko, Y. L.; Yaminsky, I. V., Comparative studies of bacteria with an atomic force microscopy operating in different modes. *Ultramicroscopy* **2001,** *86* (1–2), 121-128.
38. Allison, D. P.; Sullivan, C. J.; Mortensen, N. P.; Retterer, S. T.; Doktycz, M., Bacterial Immobilization for Imaging by Atomic Force Microscopy. **2011,** (54), e2880.
39. Limunus amebocyte lysate. http://www.acciusa.com/pdfs/accProduct/pisheets/Chromo-LAL%20Insert%20English.pdf.
40. LPS Elisa Kit. https://www.abbkine.com/product/mouse-lipopolysaccharides-lps-elisa-kit-kte71161/.

"For TOC only"